spectively. This observation suggests interactions of the respective vanadyl carrier complexes with biological recognition sites with more effective release of vanadyl ions from the L-enantiomeric complexes. Experiments aimed at identifying the sites of action(s) of intracellular vanadyl are in progress as are in vivo studies of the most potent agents.

ACKNOWLEDGMENTS

The secretarial assistance of Dalia Ganiel and Rona Levin is gratefully acknowledged. Y.S. is the incumbent of the C. H. Hollenberg Chair in Metabolic and Diabetes Research established by the Friends and Associates of Dr. C. H. Hollenberg of Toronto, Canada. A. Shanzer is the holder of the Siegfried and Irma Ullmann Professorial Chair.

REFERENCES

Becker, B. A., & Roth, R. A. (1990) *Ann. Res. Med. 41*, 99-115.
Boas, L. F. V., & Pessoa, J. C. (1987) in *Comprehensive Coordination Chemistry* (Wilkinson, Sir J., Ed.) Vol. 3, p 487, Pergamon Press, Oxford.
Butler, A. (1990) in *Vanadium in Biological Compounds* (Chasteen, N. D., Ed.) pp 25-49, Kluwer Academic Publishers, Dordrecht.
Degani, H., Gochin, M., Karlish, S. J. D., & Shechter, Y. (1981) *Biochemistry 20*, 5795-5799.
Dodge, R. P., Templeton, D. H., & Zalkin, A. (1961) *J. Phys. Chem. 35*, 55.
Fisher, D. C., Barclay-Peet, S. J., Balfa, C. A., & Raymond, K. N. (1989) *Inorg. Chem. 28*, 4399-4406.
Green, A. (1986) *Biochem. J. 238*, 665-669.
Heyliger, C. E., Tahilliani, A. G., & McNeill, J. H. (1985) *Science 227*, 1474-1476.
Hirosova, D., & Koldovsk, O. (1969) *Physiol. Bohemoslov, 18*, 281-284.
Macara, I. G. (1980) *Trends Biochem. Sci. 5*, 92-94.
Meyerovitch, J., Farfel, Z., Sack, Y., & Shechter, Y. (1987) *J. Biol. Chem. 262*, 6658-6662.
Meyerovitch, J., Rothenberg, P., Shechter, Y., Weir, S. A., & Kahn, C. R. (1991) *J. Clin. Invest. 87*, 1286-1294.
Moody, A. J., Stan, M. A., Stan, M., & Gliemann, J. (1974) *Horm. Metab. Res. 6*, 12-16.
Morf, W. E., Ammann, D., Bissig, L. R., Pretsch, E., & Simon, W. (1979) in *Progress in Macrocyclic Chemistry* (Izatt, R. M., & Christensen, J. J., Eds.) Vol. 1, pp 2-62, J. Wiley & Sons, New York.
Pederson, R. A., Ramanadham, S., Buchan, A. M. J., & McNeill, J. H. (1989) *Diabetes 38*, 1390-1395.
Ramanadham, S., Brownsey, R. W., Cross, G. H., Mongold, J. J., & McNeil, J. H. (1989) *Metabolism 38*, 1022-1028.
Reddy, S. S.-K., & Kahn, S. R. (1988) *Diabetes Medicine 5*, 621-629.
Rodbell, M. (1964) *J. Biol. Chem. 239*, 375-380.
Rossetti, L., & Laughlin, M. R. (1989) *J. Clin. Invest. 84*, 892-899.
Shechter, Y. (1990) *Diabetes 39*, 1-5.
Shechter, Y., & Karlish, S. J. D. (1980) *Nature (London) 284*, 556-558.
Simons, T. J. B. (1979) *Nature (London) 281*, 337-338.
Tamura, S., Brown, T. A., Whipple, J. H., Yamaguchi, Y. F., Dubler, R. E., Cheng, K., & Larner, J. (1984) *J. Biol. Chem. 259*, 6650-6658.
Tor, Y., Libman, J., & Shanzer, A. (1987) *J. Am. Chem. Soc. 109*, 6518-6519.
Waters, M. D. (1977) *Adv. Med. Toxicol. 2*, 147-189.

^{1}H NMR Assignment and Secondary Structure of the Cell Adhesion Type III Module of Fibronectin†

Martin Baron,‡ Alison L. Main,‡ Paul C. Driscoll,‡ Helen J. Mardon,§ Jonathan Boyd,‡ and Iain D. Campbell*,‡

Department of Biochemistry, University of Oxford, South Parks Road, Oxford OX1 3QU, U.K., and Sir William Dunn School of Pathology, University of Oxford, Oxford OX1 3RE, U.K.

Received August 27, 1991; Revised Manuscript Received November 6, 1991

ABSTRACT: The secondary structure of the tenth type III module from human fibronectin has been determined using NMR. This type of module appears many times in a wide variety of proteins. The type III module described here contains an Arg-Gly-Asp sequence known to be involved in cell–cell adhesion. The module was expressed in yeast and characterized by amino acid sequencing and mass spectrometry. 2D and 3D NMR spectroscopy of ^{15}N-labeled protein was used to perform sequence-specific assignment of the spectrum. The secondary structure was defined by patterns of nuclear Overhauser effects, $^3J_{NH\text{-}\alpha CH}$ spin–spin coupling constants, and amide proton solvent exchange rates. The molecule consists of seven β-strands in two antiparallel β-sheets with an immunoglobulin-like fold similar to that predicted for homologous modules in the cytokine receptor super family [Bazan, J. F. (1990) *Proc. Natl. Acad. Sci. U.S.A. 87*, 6934-6938]. The Arg-Gly-Asp sequence is located on a loop between the β-strands F and G.

Fibronectin, a large protein found in the extracellular matrix and the serum, is made up of three different kinds of structural units, usually called types I–III (Ruoslahti, 1988). In this respect it is similar to many proteins that have evolved by exon shuffling and duplication of a limited number of autonomously folding structural units, or modules (Patthy, 1991; Baron et al., 1991). The diverse biological roles of fibronectin have been extensively studied (Hynes, 1990). It is found in serum, where it binds to both fibrin blood clots and platelets, and is also a major component of the extracellular matrix which provides anchorage sites for cells and thus helps maintain the integrity of tissues. Fibromectin plays a key role in wound healing and embryonic development since it binds to other components of

† This is a contribution from the Oxford Centre for Molecular Sciences, which is supported by SERC and MRC. P.C.D. is supported by a Royal Society University Research Fellowship.
‡ Department of Biochemistry, University of Oxford.
§ Sir William Dunn School of Pathology, University of Oxford.

0006-2960/92/0431-2068$03.00/0

the extracellular matrix and to receptors on the cell surface, thus facilitating organized cell migration. No crystal structures of either the intact molecule or fragments of fibronectin are known. However, the solution structures of an expressed type I module from fibronectin (Baron et al., 1990b) and a homologous type II module from the bovine seminal fluid protein PDC-109 (Constantine et al., 1991) have been determined recently using NMR[1] techniques. In this paper we describe an NMR study of a type III module from human fibronectin.

The type III module is characterized by a consensus sequence of conserved amino acids which is approximately 90 residues in length. Plasma fibronectin contains 15 type III repeats per monomer, while cellular fibronectin may contain one or two additional type III modules, due to alternative splicing of the pre-mRNA, depending on the cell type (Ruoslahti, 1988). The type III module is also found in numerous other extracellular, cell surface, and muscle-associated proteins (Moos et al., 1988; Bazan, 1990; Labeit et al., 1990). Thus a knowledge of the structure of one example will prove useful in modeling the structure of many other proteins. Using proteolytic fragments of fibronectin and synthetic peptides, a cell adhesion site has been localized to an Arg-Gly-Asp sequence lying close to the C-terminus of the tenth type III module of fibronectin (Pierschbacher & Ruoslahti, 1984). The Arg-Gly-Asp sequence has been found to have general significance for cell adhesion, being a recognition site for binding to the integrin family of receptors (D'Souza et al., 1991). Not all Arg-Gly-Asp-containing proteins bind to integrins, however, and this suggests that the conformation and dynamics of this sequence are important for its recognition. Knowledge of the conformation of this sequence within the context of the type III module is thus of considerable interest. As a first stage toward the determination of the 3D structure of the type III module in solution we have obtained virtually complete assignment of the ^1H and ^{15}N NMR spectra and have determined the secondary structure of the tenth type III module of fibronectin, corresponding to residues 1416–1509 of human fibronectin (Kornblihtt et al., 1985) and referred to in this paper as residues 1–94.

Materials and Methods

Vector Construction. A yeast secretion system based on the α factor leader sequence was used to express the type III module into the yeast culture medium from which it could readily be purified. The general strategy for the expression of protein modules has been described previously (Baron et al., 1990a).

A DNA fragment coding for residues 1416–1509 of human fibronectin was obtained by using the polymerase chain reaction. Amplification was from a single-stranded cDNA hepatocyte cell library. The 5′ primer oligonucleotide had the sequence GTTTCTGATGTTCCGAGGGA, and the 3′ primer had the sequence ATTAGGATCCTTATGTGGACTGGGTTCCAATCA. The latter had a 3′ noncomplementary sequence encoding a stop translation codon and a *Bam*HI site. Amplification was performed on a Perkin-Elmer PCR machine for 25 cycles. Each cycle consisted of a 1-min melting step at 94 °C, a 1-min step at 56 °C for annealing, and a 3-min primer extension step at 72 °C. Primer extension was performed using *Thermus aquaticus* polymerase supplied by Boehringer Mannheim. The fragment was cut with *Bam*HI and ligated into the vector pMB50 that had been cut with *Stu*I and *Bam*HI. This placed the type III module sequence in frame, with the sequence encoding the yeast α factor leader sequence immediately after the codon encoding the Arg residue that forms the cleavage site for the *Kex2* enzyme. A single clone was sequenced in both directions using primers complementary to pMB50 sequences just 5′ and 3′ to the insert. A *Bgl*II/*Bam*HI fragment encoding the leader/module fusion was then purified and ligated into the *Bgl*II site of the yeast expression plasmid pMA91 (Mellor et al., 1983) to give the plasmid pMA91/F3.

Yeast Transformation, Expression, and Purification of Protein. Competent yeast cells (*Saccharomyces cerevisae* MD50/a,α/leu2,3) were transformed with pMA91/F3 (Beggs, 1978). Transformed cells were selected by their ability to grow on media lacking leucine. One-liter cultures were grown for 60 h in yeast nitrogen base medium without amino acids (supplied by Difco), using rotary shaking incubators at 30 °C. The culture was supplemented with 5 mL of 40% glucose solution at 0, 24, and 48 h. To obtain ^{15}N-labeled material, yeast nitrogen base without amino acids and ammonium sulfate was supplemented with 0.5 g/L ^{15}N-labeled ammonium sulfate (suppled by MSD Isotopes). C18 reverse-phase beads (supplied by HPLC technology) were included in the culture medium. They were recovered at the end of the incubation by filtering the culture through a no. 2 glass scinter. The beads were washed with water, then transferred to a 60% acetonitrile/0.1% trifluoroacetic acid (TFA) solution, and shaken for 30 min. The beads were then removed by filtration. The filtrate was lyophilized, resuspended in a small volume of water, and centrifuged several times to remove insoluble material before being applied to a C8 reverse-phase HPLC column. The module was eluted by an acetonitrile gradient in 0.1% TFA. The protein was further purified by cation-exchange HPLC, using a pH gradient, and was finally passed down the C8 reverse-phase HPLC column.

Characterization of Purified Protein. Purified type III module was sequenced by automated Edman degradation in an Applied Biosystems 470A protein gas-phase sequencer with on line PTH analysis for 10 cycles. The molecular weight was measured by injecting a solution of the protein into the electrospray system of a VG BIO Q quadrupole mass spectrometer.

Biological Activity. The functional integrity of the type III module was tested using an assay to monitor the inhibition of cell-spreading of baby hamster kidney fibroblasts (BHK cells). This assay is routinely used to quantitate the biological activity of fibronectin peptides or proteolytic fragments containing cell binding motifs (Humphries et al., 1986; Yamada & Kennedy, 1984). The peptides used in the assay were the type III module, Gly-Arg-Gly-Asp-Ser (GRGDS), and a recombinant protein comprising the third and fourth fibronectin type I module pair. Minor modifications of the assay protocol were as follows: 6.4-mm wells in 96-well tissue culture plates (Falcon U.K.) were preincubated with 100 μL of 5 μg/mL human plasma fibronectin (Sigma). BHK cells (1.5×10^4) in 75 μL of minimal essential medium were added to each well, with 25 μL of protein solution in phosphate-buffered saline. Each protein concentration was tested in duplicate. The percentage of cells with a well-spread morphology was assessed after 60-min incubation. In three independent experiments, 300 cells in each well were counted using phase-contrast microscopy.

NMR Analysis. Purified fibronectin type III module was dissolved in either D_2O or 90% H_2O/10% D_2O to a concentration of approximately 3 mM, and the pH was adjusted to 4 (uncorrected meter readings were used in the case of D_2O

[1] Abbreviations: NMR, nuclear magnetic resonance; NOE, nuclear Overhauser effect; PCR, polymerase chain reaction; RGD, Arg-Gly-Asp; TFA, trifluoroacetic acid.

samples). ^1H NMR experiments were recorded on Bruker AM600 (600 MHz ^1H) and AM500 MHz ^1H) spectrometers at temperatures of 39 and 47 °C. Double quantum filtered (DQF) correlation spectra (Rance et al., 1983) and nuclear Overhauser effect (NOE) spectra (Kumar et al., 1981) were recorded in a phase-sensitive manner using the time-proportional phase increment method for sign discrimination in the F_1 dimension. Mixing times of 50, 160, and 200 ms were used for NOESY experiments. Homonuclear Hartmann–Hahn (HOHAHA) spectra were collected using the WALTZ-17 mixing sequence (Bax et al., 1987) with a mixing time of approximately 50 ms. For spectra collected in D_2O, irradiation of the solvent resonance was carried out during the relaxation delay. In the case of NOE and HOHAHA spectra recorded in 90% H_2O/10% D_2O, a "jump return" sequence (Plateau & Gueron, 1982) was used to suppress the solvent resonance. The receiver phase was adjusted to eliminate base-line distortions (Marion & Bax, 1988). Amide hydrogens that were relatively slow to exchange with solvent were identified by lyophilizing a sample in 100% H_2O and resuspending in D_2O before recording a NOESY spectrum. Heteronuclear ^1H–^{15}N experiments were recorded on a home-built spectrometer (500-MHz ^1H 50.7-MHz ^{15}N) at a temperature of 39 °C. A heteronuclear ^{15}N–^1H single quantum correlation spectrum (HSQC) (Bodenhausen & Ruben, 1980; Norwood et al., 1990) was acquired to correlate amide ^1H and ^{15}N chemical shifts. For the measurement of $^3J_{NH\text{-}\alpha CH}$ spin–spin coupling constants, a ^1H-detected heteronuclear ^1H–^{15}N multiple quantum correlation spectrum (HMQC-J) was recorded. The coupling constants were extracted by fitting F_1 traces of this spectrum to a theoretical line shape (Kay & Bax, 1990). Three-dimensional (3D) heteronuclear ^1H-HOHAHA-^{15}N-^1H-HMQC and 3D ^1H-NOESY-^{15}N-^1H-HMQC experiments were also performed. For the 3D spectra, the water signal was suppressed using spin lock purge pulses during the application of the heteronuclear pulse sequence (Messerle et al., 1989). The 3D spectra were recorded with 32 increments in the ^{15}N (F_2) dimension and 128 increments in the ^1H (F_1) dimension. The sweep widths in the F_1 and F_2 dimensions were set so as to maximize digital resolution in the processed spectrum. The initial t_1 and t_2 delays were set to be exactly half a dwell time (Bax et al., 1991). In the ^{15}N dimension two outlying amide NH signals were "folded" and appeared as peaks of opposite phase. Sign discrimination in the F_1 and F_2 dimensions was achieved using hypercomplex acquisition. The data were processed to yield a final pure absorption matrix of size 256 × 64 × 512 data points. For all spectra recorded in 90% H_2O/10% D_2O, the residual water signal was removed by deconvolution in the time domain (Marion et al., 1989). All spectra were processed using FELIX processing software (Hare Research Inc., Washington).

Results

Expression of the Type III Module. Following batch adsorption from the culture medium the expressed module was found to be the major protein peak eluting from the initial reverse-phase HPLC C8 column. Cation-exchange HPLC was used to remove a small amount of material which had an extra arginine at the N-terminus due to incorrect processing of the leader peptide. N-Terminal sequence analysis and electrospray mass spectrometry confirmed the identity of the product with a molecular weight of 9938.

Biological Activity. The results of the biological assay are shown in Figure 1. Forty percent inhibition of BHK cell-spreading was achieved by similar molar concentrations of the type III module (1 mM) and GRGDS (1.8 mM). At the same concentration, the fibronectin type I module pair had no effect on cell-spreading. Thus, the assay performed clearly shows that the expressed type III module is functionally active and inhibits cell binding to intact fibronectin.

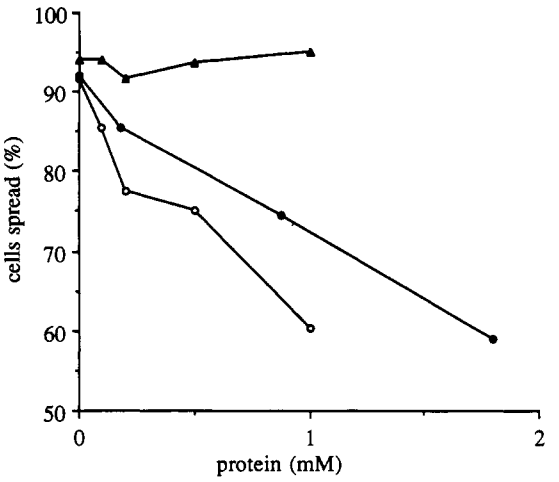

FIGURE 1: Biological activity of type III. Inhibition of BHK cell-spreading by type III (closed circles), GRGDS (open circles), or a type I module pair (triangles) on tissue culture plastic precoated with 5 μg/mL fibronectin. The type I module pair, a protein of similar molecular weight to type III, does not contain the cell binding motif (RGD) and has no effect on cell-spreading.

NMR Analysis. Sequence-specific assignment of the NMR spectrum was carried out using established methodology (Wüthrich, 1986). 2D HOHAHA and DQF COSY spectra were used to identify spin systems which were then assigned sequence specifically via sequential NOEs and the known primary sequence. The assignment was assisted by heteronuclear (^{15}N–^1H) 3D HOHAHA and NOESY experiments which resolved overlapped amide protons. Figure 2 shows strips from a 3D heteronuclear NOESY experiment. Each strip is a small section taken from the $^1H(F_3)$–$^1H(F_1)$ plane of the 3D matrix, which exhibits the cross-peaks of maximum intensity for the chosen NH proton. The strips are arranged in sequential order and illustrate the assignment of two regions of the protein. Virtually complete assignment of the spectrum has been achieved by these methods, and a table of assignments is included in the supplementary material. The sequential NOEs observed are shown in Figure 3 together with the $^3J_{HN\text{-}\alpha CH}$ coupling constants and the amide protons that exchanged slowly in D_2O. Strong $C^\alpha H(i)$–$NH(i+1)$ NOEs provide evidence of an extended structure such as that found in a β-sheet, and strong $NH(i)$–$NH(i+1)$ NOEs are evidence of helical or turn conformations. These are associated with large (>7-Hz) and small (<6-Hz) $^3J_{HN\text{-}\alpha CH}$ coupling constants, respectively (Wüthrich, 1986).

The patterns of sequential NOEs, slowly exchanging amides, coupling constants, slowly exchanging amide hydrogens, and interstrand NOEs are consistent with seven β-strands organized into two antiparallel β-sheets of three and four strands as shown in Figure 4. The triple-stranded β-sheet consists of residues Leu8 to Thr14, Ser17 to Trp22, and Ser55 to Ser60. Val11 in strand A is in a β-bulge. A hairpin turn occurs between residues Thr14 and Ser17 with a proline at position 15. The four-stranded antiparallel β-sheet consists of residues Gln46 to Val50, Tyr31 to Thr39, Val66 to Val75, and Ile88 to Thr94. The topology of the β-strands is given in Figure 5.

Discussion

The secondary structure, which is illustrated in Figure 5, contains two antiparallel β-sheets which are composed of three

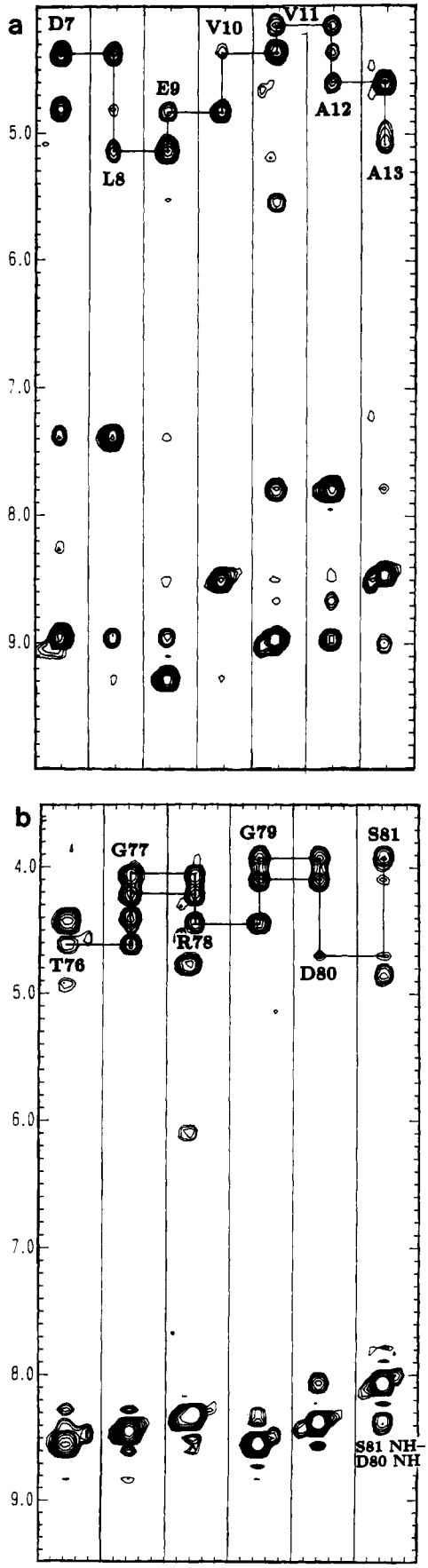

FIGURE 2: 3D NMR strip plots. Each strip corresponds to an assigned amide ^{15}N resonance in a 3D NOESY-^{15}N-^{1}H-HMQC experiment. Labeled cross-peaks are the intraresidue $C^{\alpha}H$–HN NOEs, and these are connected with horizontal and vertical lines via sequential $C^{\alpha}H$-(i)–NH(i + 1) NOEs. (a) Sequential assignment of β-strand A. (b) Sequential assignment through the Arg-Gly-Asp cell adhesion site.

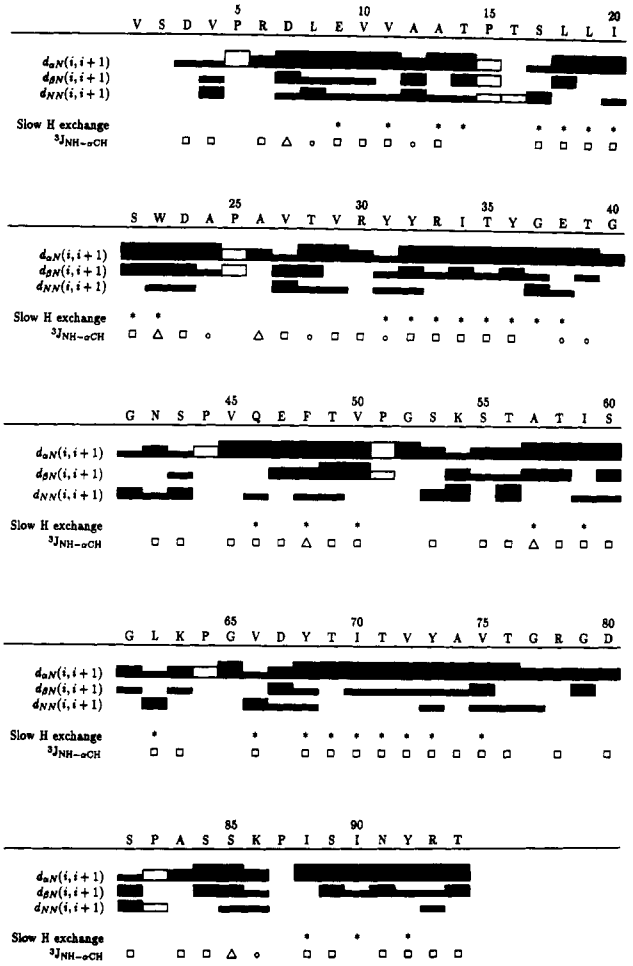

FIGURE 3: Summary of sequential NOEs, slowly exchanging amides, and $^{3}J_{HN\text{-}\alpha CH}$ coupling constants. The bar heights correspond to the relative strengths of the NOEs (strong, medium, and weak) and are placed under residue (i + 1). Open boxes represent NOEs involving proline $C^{\delta}H$ atoms. (*) marks amide protons considered to be slowly exchanging. Circles represent $^{3}J_{HN\text{-}\alpha CH}$ coupling constants that are <6 Hz, triangles, 6–7 Hz, and squares, >7 Hz.

(A, B, E) and four (C, D, F, G) β-strands, respectively. This is reminiscent of the topology found in immunoglobulin C domains (Williams & Barclay, 1988). In the type III module, however, strand D is hydrogen bonded to strand C rather than strand E. This is a similar topology to that described for the D2 domain of the T cell CD4 protein (Ryu et al., 1990) and for the bacterial chaperone protein PapD (Holmgren & Brändén, 1989).

The positions of residues that are highly conserved in type III modules are also indicated in Figure 5. These conserved residues fall into two blocks of strong sequence homology separated by a highly variable sequence of about 20 residues (Bazan, 1990). The β-strands A–C and F have highly conserved hydrophobic residues every second residue. The loop between strands E and F is also well conserved.

The RGD cell adhesion site lies in a turn between strands F and G of the major β-sheet and in the single module is thus solvent exposed as would be expected for its cell adhesion function. Our preliminary 3D structural analysis indicates that the RGD loop is not well-defined with respect to the rest of the molecule. It is positioned on the same side of the module as the N-terminus and is likely to lie at the domain–domain interface between the ninth and tenth type III modules. This is interesting in the light of experiments showing that full activity of the RGD site requires the presence of sequences N-terminal to the tenth type III module. This second site has

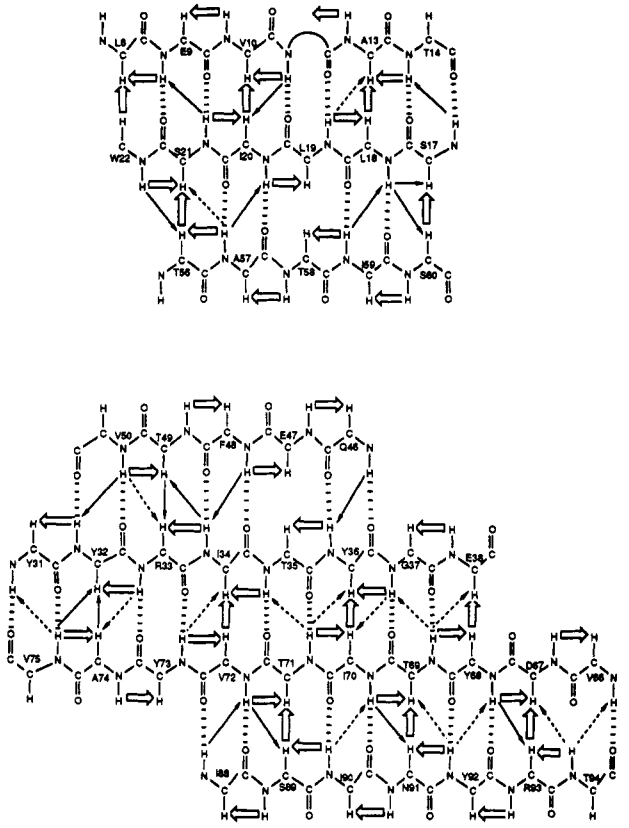

FIGURE 4: Secondary structure. The secondary structure of the type III module deduced from NOE, $^3J_{HN\text{-}\alpha CH}$ spin–spin coupling constant, and slow exchanging amide data. The various strengths of NOEs are represented as follows: strong NOEs, large open arrows; medium NOEs, solid arrows; weak NOEs, broken arrows. Dashed lines represent predicted hydrogen bonds consistent with the slow exchanging amide data. Expected $C^{\alpha}H$–$C^{\alpha}H$ NOEs are not observed for E47 to T35 and T58 to L19. In both cases the chemical shifts of the two $C^{\alpha}H$ protons are too close together for cross-peaks to be observed.

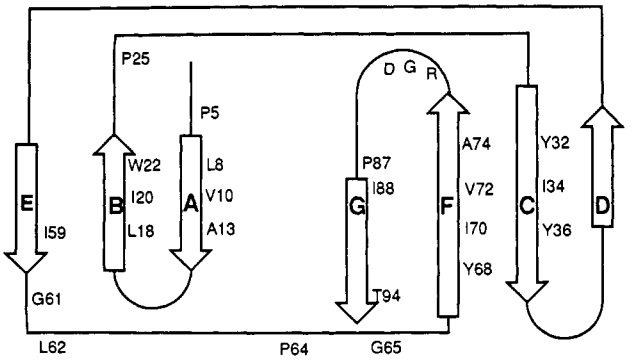

FIGURE 5: Schematic diagram showing the topology of β-strand connections. Open arrows represent β-strands labeled A–G. The residues that are highly conserved in type III modules are indicated with one-letter codes and residue number. The approximate location of the Arg-Gly-Asp cell adhesion site is indicated by RGD.

been mapped to a region within the eighth and ninth type III repeats (Obara et al., 1988). Structure determination of the ninth and tenth modules as a pair will thus be of interest.

The secondary structure of the type III module described here can be compared with that previously predicted for homologous type III sequences found in the cytokine receptor superfamily (Bazan, 1990). By analyzing homologous type III sequences, the positions of conserved hydrophobic residues, and known disulfide bond patterns, Bazan correctly predicted the locations and topology of secondary structure elements although some minor deviations such as the β-bulge in strand A were not identified. It is interesting to note that the conserved WSxWS sequence which is often found in the type III modules of cytokine receptors proximal to the membrane-spanning segment is predicted to be in the same region of the molecule as the RGD loop.

A detailed analysis of the 3D structure of the type III module is now underway in this laboratory. Initial results from simulated annealing protocols [see Driscoll et al. (1991)] indicate that the two β-sheets of three and four strands are stacked on top of one another, enclosing a hydrophobic core. The refined 3D structure will yield more information about the loop containing the RGD sequence and consequently will provide an insight into the mechanism of cell binding to fibronectin. Knowledge of the tertiary structure will help to improve sequence alignment of type III modules and aid homology modeling of proteins containing such modules.

ACKNOWLEDGMENTS

We thank Alexander Steinkasserer for the hepatocyte cDNA library and assistance with PCR, Kath Nolan for introducing a *StuI* site into pMB50, Kate Exton for her excellent technical support, Robin Aplin for the mass spectrometry results, and Tony Willis for the protein sequencing. The yeast strain MD50 was a gift from British Biotechnology.

SUPPLEMENTARY MATERIAL AVAILABLE

Table of assignments and chemical shift data for ^1H spectra obtained at 47 °C (6 pages). Ordering information is given on any current masthead page.

REFERENCES

Baron, M., Kingsman, A. J., Kingsman, S. M., & Campbell, I. D. (1990a) *Protein Production in Biotechnology* (Harris, T. J. R., Ed.) pp 49–60, Elsevier, London.

Baron, M., Norman, D., Willis, A. J., & Campbell, I. D. (1990b) *Nature 345*, 642–646.

Baron, M., Norman, D. G., & Campbell, I. D. (1991) *Trends Biochem. Sci. 16*, 13–17.

Bax, A., Sklenar, V., Clore, G. M., & Gronenborn, A. M. (1987) *J. Am. Chem. Soc. 109*, 6511–6513.

Bax, A., Ikura, M., Kay, L. E., & Zhu, G. (1991) *J. Magn. Reson. 91*, 174–178.

Bazan, J. F. (1990) *Proc. Natl. Acad. Sci. U.S.A. 87*, 6934–6938.

Beggs, J. D. (1978) *Nature 275*, 104–109.

Bodenhausen, G., & Ruben, D. J. (1980) *Chem. Phys. Lett. 69*, 185–189.

Constantine, K. L., Ramesh, V., Banyai, L., Trexler, M., Patthy, L., & Llinas, M. (1991) *Biochemistry 30*, 1663–1672.

Driscoll, P. C., Clore, G. M., Marion, D., Wingfield, P. T., & Gronenborn, A. M. (1990) *Biochemistry 29*, 3542–3556.

Driscoll, P. C., Cyster, J. G., Campbell, I. D., & Williams, A. F. (1991) *Nature 353*, 762–765.

D'Souza, S. E., Ginsberg, M. H., & Plow, E. F. (1991) *Trends Biochem. Sci. 16*, 246–250.

Holmgren, A., & Bränden, C. I. (1989) *Nature 342*, 248–251.

Humphries, M. J., Akiyama, S. K., Komoriya, A., Olden, K., & Yamada, K. M. (1986) *J. Cell Biol. 103*, 2637–2647.

Hynes, R. O. (1990) *Fibronectins*, Springer Verlag, Berlin.

Hynes, R. O., & Yamada, K. M. (1982) *J. Cell Biol. 95*, 369–377.

Kay, L. E., & Bax, A. (1990) *J. Magn. Reson. 86*, 110–126.

Kornblihtt, A. R., Umezawa, K., Vibe-Pedersen, K., & Baralle, F. E. (1985) *EMBO J. 4*, 1755–1759.

Kumar, A., Ernst, R. R., & Wüthrich, K. (1981) *Biochem. Biophys. Res. Commun. 95*, 1–6.

Labeit, S., Barlow, D. P., Gautel, M., Gibson, T., Holt, J., Hsieh, C. L., Francke, U., Leonard, K., Wardale, J., Whiting, A., & Trinick, J. (1990) *Nature 345*, 272–276.
Marion, D., & Bax, A. (1988) *J. Magn. Reson. 79*, 352–356.
Marion, D., Ikura, M., & Bax, A. (1989) *J. Magn. Reson. 84*, 425–430.
Mellor, J., Dobson, M. J., Roberts, N. A., Tuite, M. F., Emtage, J. S., White, S., Lowe, P. A., Patel, T., Kingsman, A. J., & Kingsman, S. M. (1983) *Gene 24*, 1–14.
Messerle, B. A., Wider, G., Otting, G., Weber, C., & Wüthrich, K. (1989) *J. Magn. Reson. 85*, 608–613.
Moos, M., Tacke, R., Scherer, H., Teplow, D., Früh, K., & Schachner, K. (1988) *Nature 334*, 701–703.
Norwood, T. J., Boyd, J., Heritage, J. E., Soffe, N., & Campbell, I. D. (1990) *J. Magn. Reson. 87*, 488–501.
Obara, M., Kang, M. S., & Yamada, K. M. (1988) *Cell 53*, 649–657.
Patthy, L. (1991) *Curr. Opin. Struct. Biol. 1*, 351–361.
Pierschbacher, M. D., & Ruoslahti, E. *Nature 309*, 30–33.
Plateau, P., & Gueron, M. (1982) *J. Am. Chem. Soc. 104*, 7310–7311.
Rance, M., Sorensen, O. W., Bodenhausen, G., Wagner, G., Ernst, R. R., & Wüthrich, K. (1983) *Biochem. Biophys. Res. Commun. 117*, 479–485.
Ruoslahti, E. (1988) *Annu. Rev. Biochem. 57*, 375–413.
Ryu, S. E., Kwong, P. D., Truneh, A., Porter, T. G., Arthos, J., Rosenberg, M., Dai, X., Xuong, N., Axel, R., Sweet, R. W., & Hendrickson, W. A. (1990) *Nature 348*, 419–425.
Williams, A. F., & Barclay, N. (1988) *Annu. Rev. Immunol. 6*, 381–405.
Wüthrich, K. (1986) *NMR of Proteins and Nucleic Acids*, Wiley-Interscience, New York.
Yamada, K. M., & Kennedy, D. W. (1984) *J. Cell Biol. 99*, 29–36.

$^{14,15}N$, ^{13}C, ^{57}Fe, and $^{1,2}H$ Q-Band ENDOR Study of Fe–S Proteins with Clusters That Have Endogenous Sulfur Ligands†

Andrew L. P. Houseman,‡ Byung-Ha Oh,§ Mary Claire Kennedy,∥ Chaoliang Fan,‡ Melanie M. Werst,‡ Helmut Beinert,∥ John L. Markley,§ and Brian M. Hoffman*,‡

Department of Chemistry, Northwestern University, 2145 Sheridan Road, Evanston, Illinois 60208-3113, Department of Biochemistry, College of Agriculture and Life Sciences, University of Wisconsin—Madison, 420 Henry Hall, Madison, Wisconsin 53706, and Department of Biochemistry and National Biomedical ESR Center, Medical College of Wisconsin, 8701 Watertown Plank Road, Milwaukee, Wisconsin 53226

Received August 23, 1991; Revised Manuscript Received November 8, 1991

ABSTRACT: The benefits of performing ENDOR experiments at higher microwave frequency are demonstrated in a Q-band (35 GHz) ENDOR investigation of a number of proteins with [*n*Fe–*m*S] clusters, $n = 2, 3, 4$. Each protein displays several resonances in the frequency range of 0–20 MHz. In all instances, features are seen near $\nu \approx 13$ and 8 MHz that can be assigned, respectively, to "distant ENDOR" from ^{13}C in natural-abundance (1.1%) and from ^{14}N (the $\Delta m_I = \pm 2$ transitions); the nuclei involved in this phenomenon are remote from and have negligible hyperfine couplings to the cluster. In addition, a number of proteins show local ^{13}C ENDOR signals with resolved hyperfine interactions; these are assigned to the β carbons of cysteines bound to the cluster [$A(^{13}C) \approx 1.0$ MHz]. Five proteins show resolved, local $\Delta m_I = \pm 2$ ENDOR signals from ^{14}N with an isotropic hyperfine coupling, $0.4 \lesssim A(^{14}N) \lesssim 1.0$, similar to those seen in ESEEM studies; these most likely are associated with N–H···S hydrogen bonds to the cluster. *Anabaena* ferredoxin further shows a signal corresponding to $A(^{14}N) \approx 4$ MHz. Quadrupole coupling constants are derived for both local and distant ^{14}N signals. The interpretation of the data is supported by studies on ^{15}N- and ^{13}C-enriched ferredoxin (Fd) from *Anabaena* 7120, where the ^{15}N signals can be clearly correlated with the corresponding ^{14}N signals and where the ^{13}C signals are strongly enhanced. Thus, the observation of ^{14}N $\Delta m_I = \pm 2$ signals at Q-band provides a new technique for examining weak interactions with a cluster. Six proteins show an additional pattern near $\nu \approx 18$ MHz that arises from ^{57}Fe in natural abundance (2.2%) with $A(^{57}Fe) \approx 36$ MHz, which opens the possibility of studying proteins for which enrichment is impractical. Q-band ENDOR studies also have been carried out on four ^2H-exchanged Fe–S proteins, and ENDOR detects exchangeable protons in each. The importance of these findings for the interpretation of X- and Q-band ENDOR at low radiofrequencies is discussed.

In this paper the benefits of performing ENDOR[1] experiments at higher microwave frequencies are demonstrated in a Q-band (35 GHz) ENDOR study of 10 proteins that contain [*n*Fe–*m*S] clusters, $n = 2, 3, 4$. In every case, the Q-band ENDOR spectra show proton resonances centered at $\nu(^1H) \approx 54$ MHz, but also a number of resonances in the range 0–20

† This work was supported by the National Institutes of Health (GM 34812 to H.B. and HL 13531 to B.M.H.) and the USDA (90-37120-5604 to B.M.H. and 88-37262-3406 to J.L.M.). It benefited from support by the Northwestern University Materials Research Center.
* Author to whom correspondence should be addressed.
‡ Northwestern University.
§ University of Wisconsin—Madison.
∥ Medical College of Wisconsin.

[1] Abbreviations: ENDOR, electron nuclear double resonance; EPR, electron paramagnetic resonance; ESEEM, electron spin echo envelope modulation; Fd, ferredoxin; HiPIP, high potential iron protein; NMR, nuclear magnetic resonance; RF, radio frequency; PDO, phthalate dioxygenase.

0006-2960/92/0431-2073$03.00/0